Supplemental Data

MAP18 regulates ROP2 GTPase activity during root hair growth in *Arabidopsis thaliana*

Erfang Kang, Mingzhi Zheng, Yan Zhang, Ming Yuan, Shaul Yalovsky, Lei Zhu and Ying Fu

The following supplemental materials are available.

Supplemental Figure S1. Expression level, root hairs phenotype, and localization pattern of GFP-ROP2.

Supplemental Figure S2. Expression level, root hairs phenotype, and localization pattern of MAP18-mCherry.

Supplemental Figure S3. PM-localized RIC4ΔC-GFP is significantly decreased in *map18* root hairs.

Supplemental Figure S4. Microtubules organization in *map18* mutant and *MAP18* overexpression growing root hairs.

Supplemental Figure S5. Short time treatment with taxol or phalloidin which cause microtubules or F-actin bundling but not induce phenotypic changes of root hairs.

Supplemental Figure S6. MAP18 regulation of ROP2 activity is likely independent of microtubules or F-actin.

Supplemental Figure S7. Isolation of *gdi1* knockdown and knockout mutants.

Supplemental Figure S8. MAP18 does not interact with AtRhoGDI1/SCN1 in vitro.

Supplemental Figure S9. The original full size image of Fig. 6C.

Supplemental Figure S10. The original full size image of Fig. 6G.

Supplemental Figure S11. PM-localized GFP-ROP2 is significantly decreased in *MAP18ΔN23*-overexpressing root hairs.

Supplemental Figure S12. N23 does not influence F-actin-severing activity and microtubule binding capacity of MAP18.

Supplemental Figure S13. The subcellular localization and F-actin-severing activity of MAP18 are not affected by loss of function of ROP2.

Supplemental Figure S14. N23 fragment does not bind to microtubules in vitro.

Supplemental Table S1. List of primers used in this study.

Figure S1

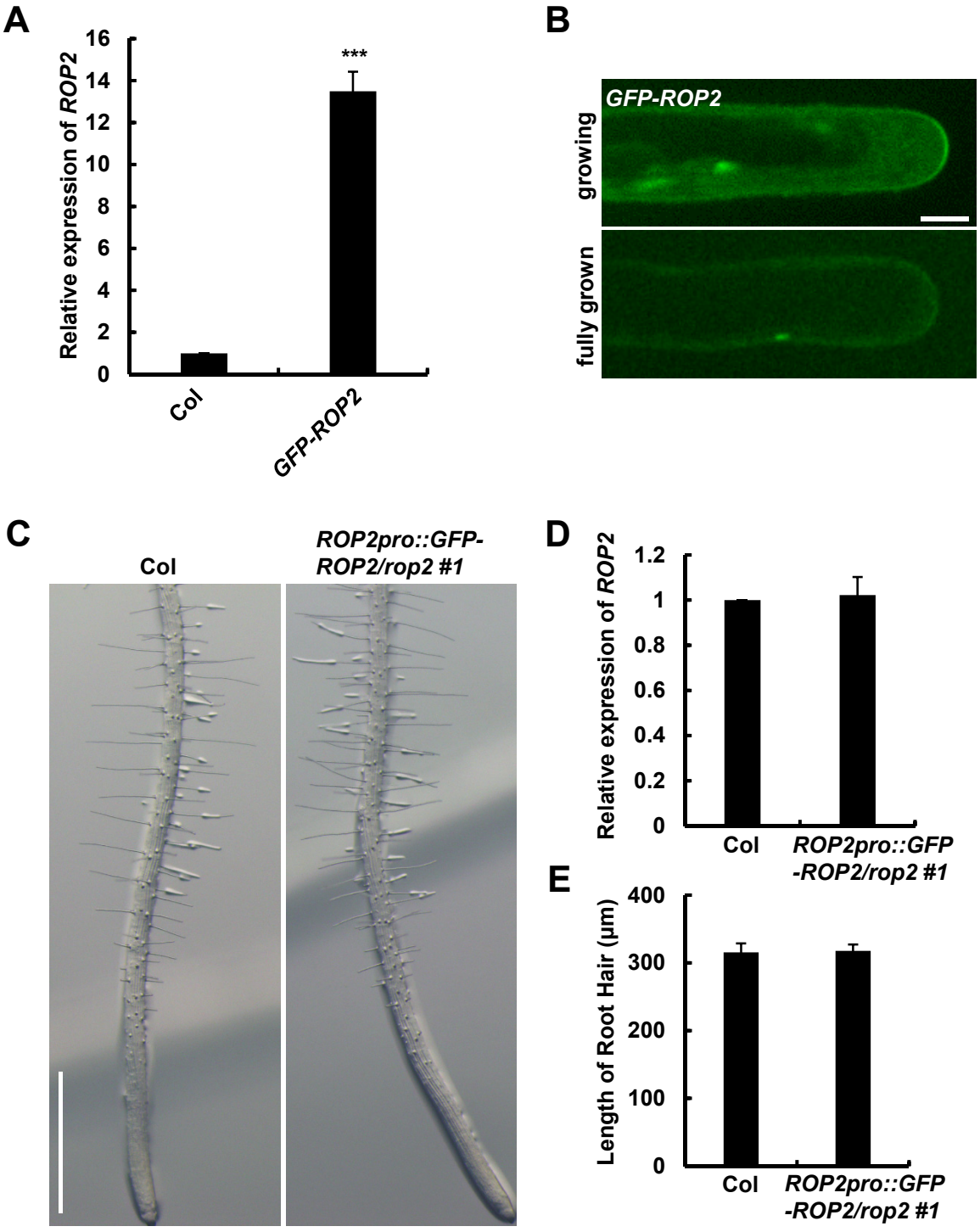
A
Relative expression of ROP2
16
14
12
10
8
6
4
2
0
***
Col
GFP-ROP2
B
GFP-ROP2
growing
fully grown
C
Col
ROP2pro::GFP-ROP2/rop2 #1
D
Relative expression of ROP2
1.2
1
0.8
0.6
0.4
0.2
0
Col
ROP2pro::GFP-ROP2/rop2 #1
E
Length of Root Hair (μm)
400
300
200
100
0
Col
ROP2pro::GFP-ROP2/rop2 #1

Supplemental Figure S1. Expression level, root hairs phenotype, and localization pattern of GFP-ROP2.

A, qRT-PCR analysis shows the relative transcript level of *ROP2* in *35S::GFP-ROP2* transgenic line (wild-type background). Data represent the mean ± SD (Standard Deviation) from at least three repeats. Relative amounts of gene expression were normalized to those of *EF1α*. ***p < 0.001 by Student's *t*-test.

B, In the growing root hairs (*35S::GFP-ROP2* transgenic line), GFP-ROP2 localized at the apical PM of hairs, but absent from the tips of fully-grown root hairs. Bar = 10 μm.

C, Representative images of root hairs from wild-type and *ROP2pro::GFP-ROP2/rop2 #1*. Bar = 1 mm.

D, qRT-PCR analysis shows that the relative transcript level of *ROP2* in *ROP2pro::GFP-ROP2/rop2 #1* was as similar as that in wild-type. Data represent the mean ± SD from at least three repeats. Relative amounts of gene expression were normalized to those of *EF1α*.

E, Statistical analysis of the average of root hairs length. The root hair length of *ROP2pro::GFP-ROP2/rop2 #1* was similar to that of wild-type. The short-root-hair defect in *rop2-1* was rescued in *ROP2pro::GFP-ROP2/rop2 #1*.

Figure S2

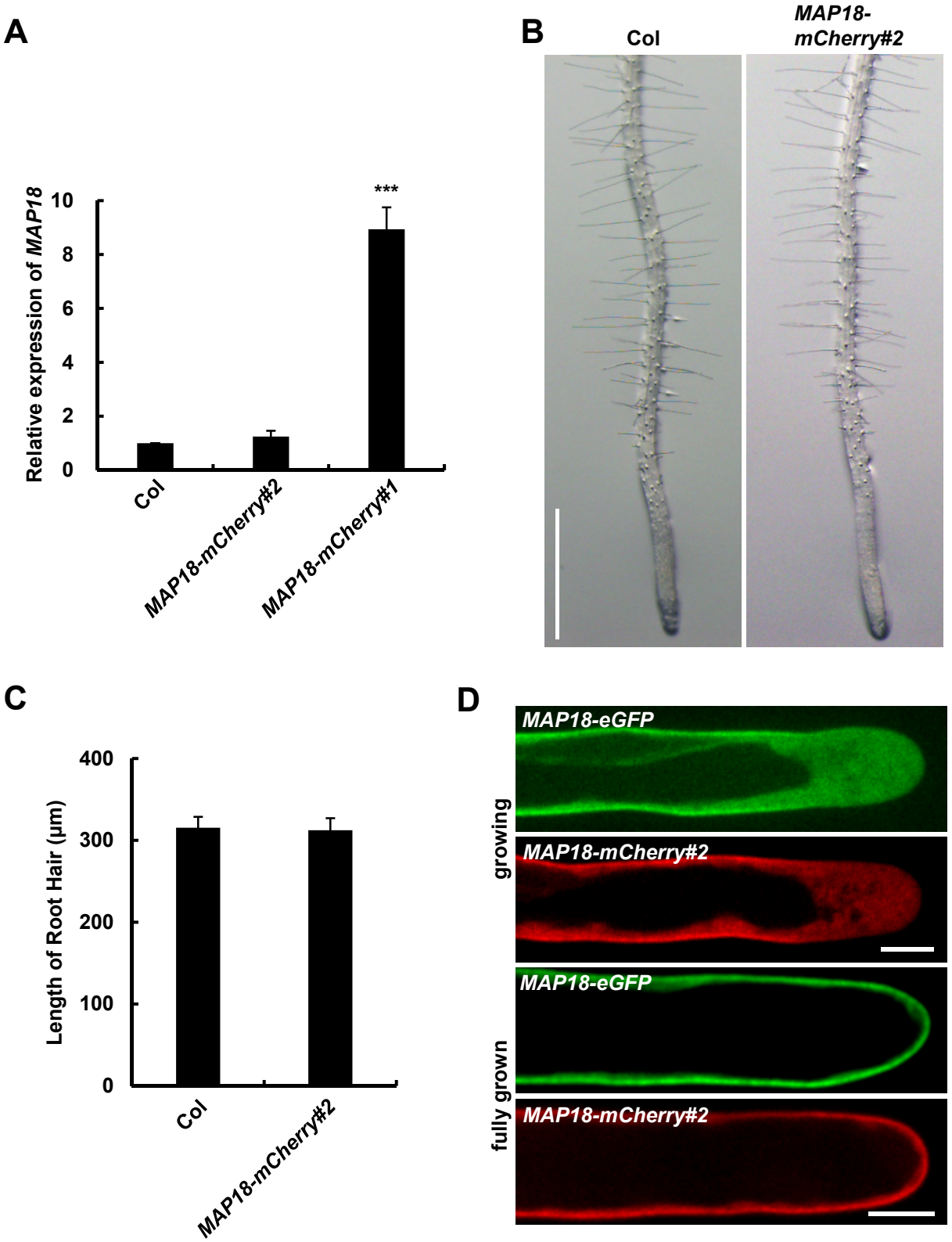
A
Relative expression of MAP18
10
8
6
4
2
0
***
Col
MAP18-mCherry#2
MAP18-mCherry#1
B
Col
MAP18-mCherry#2
C
Length of Root Hair (μm)
400
300
200
100
0
Col
MAP18-mCherry#2
D
MAP18-eGFP
MAP18-mCherry#2
growing
MAP18-eGFP
MAP18-mCherry#2
fully grown

Supplemental Figure S2. Expression level, root hairs phenotype, and localization pattern of MAP18-mCherry.

A, qRT-PCR analysis shows that the relative transcript level of *MAP18-mCherry* in transgenic lines #1 obviously exceeded that in wild-type plants, and #2 was as similar as that in wild-type. Data represent the mean ± SD from at least three repeats. Relative amounts of gene expression were normalized to those of *EF1α*. ***p < 0.001 by Student's *t*-test.

B, Representative images of root hairs from wild-type and *MAP18-mCherry#2*. Bar = 1 mm.

C, Statistical analysis of the average of root hairs length, which in *MAP18-mCherry#2* displayed as long as that of wild-type.

D, MAP18-mCherry localizes to the shank PM and the cytoplasm of the apical region of growing root hairs (upper) and throughout the entire PM of fully grown root hairs (lower) in *MAP18-mCherry#2*, as same as *MAP18-eGFP*. Bar = 10 μm.

Figure S3

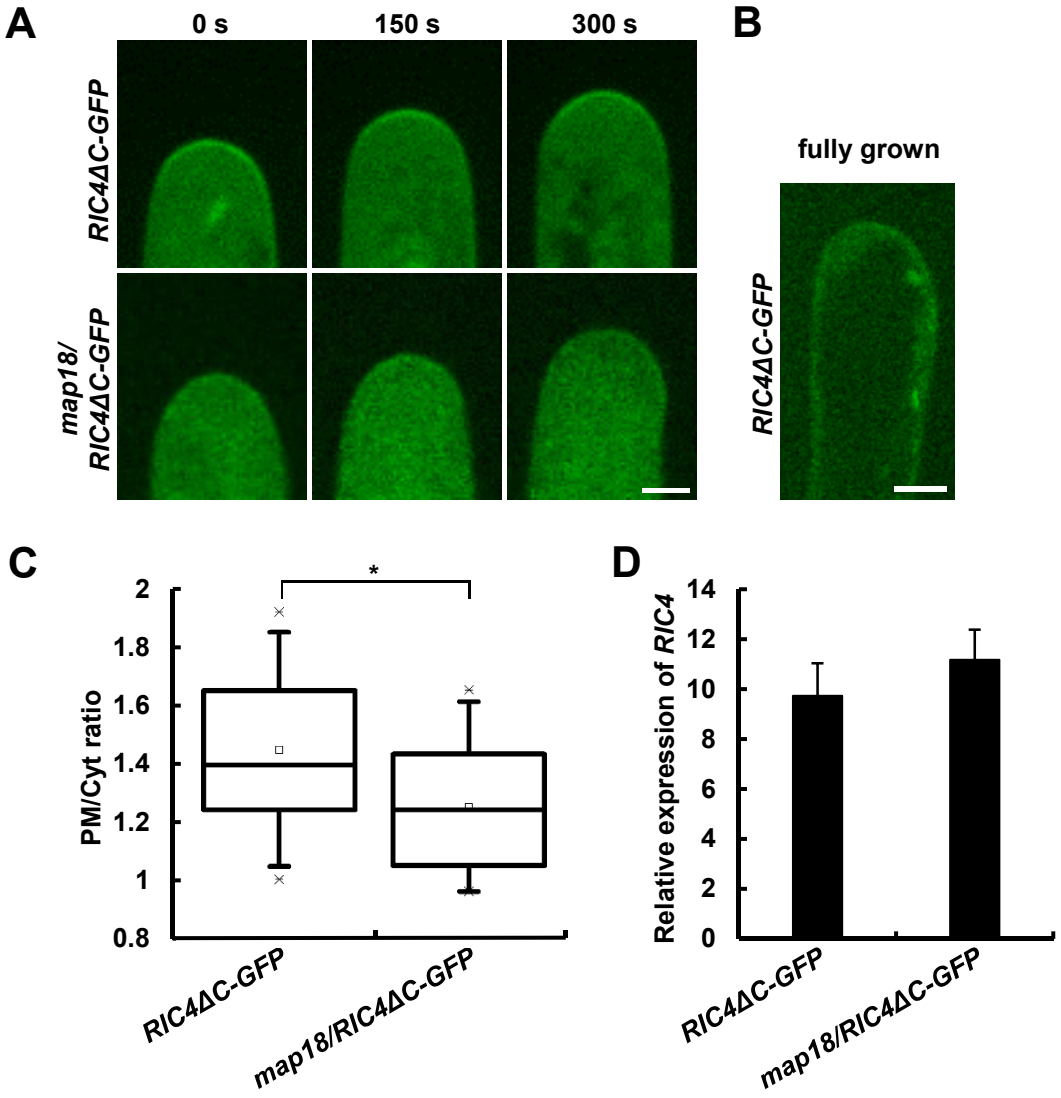
A
0 s
150 s
300 s
RIC4ΔC-GFP
map18/
RIC4ΔC-GFP
B
fully grown
RIC4ΔC-GFP
C
PM/Cyt ratio
2
1.8
1.6
1.4
1.2
1
0.8
*
RIC4ΔC-GFP
map18/RIC4ΔC-GFP
D
Relative expression of RIC4
14
12
10
8
6
4
2
0
RIC4ΔC-GFP
map18/RIC4ΔC-GFP

Supplemental Figure S3. PM-localized RIC4ΔC-GFP is significantly decreased in *map18* root hairs.

A, Time-lapse images of growing root hairs expressing RIC4ΔC-GFP in wild-type and *map18* background. PM targeting of RIC4ΔC-GFP to the tips of growing root hairs is weakened in *map18*. Bar = 5 μm.

B, RIC4ΔC-GFP disappeared at the tip when cessation of root hairs. Bar = 10 μm.

C, Quantitative analysis of RIC4ΔC-GFP fluorescence intensity PM/Cyt ratio in wild-type and *map18* mutant root hairs. Data were collected from between 36-45 root hairs from 15 roots per data set. Data are presented as box plots which reflect 25%, 50%, 75% and the maximum/minimum of total value. Asterisk (*) indicates significant difference at $p < 0.05$, ANOVA analysis.

D, qRT-PCR analysis shows that the relative transcript level of *RIC4* of transgenic lines expressing RIC4ΔC-GFP in wild-type and *map18* background was similar. Data represent the mean ± SD from at least three repeats. Relative amounts of gene expression were normalized to those of in wild-type plants.

Figure S4

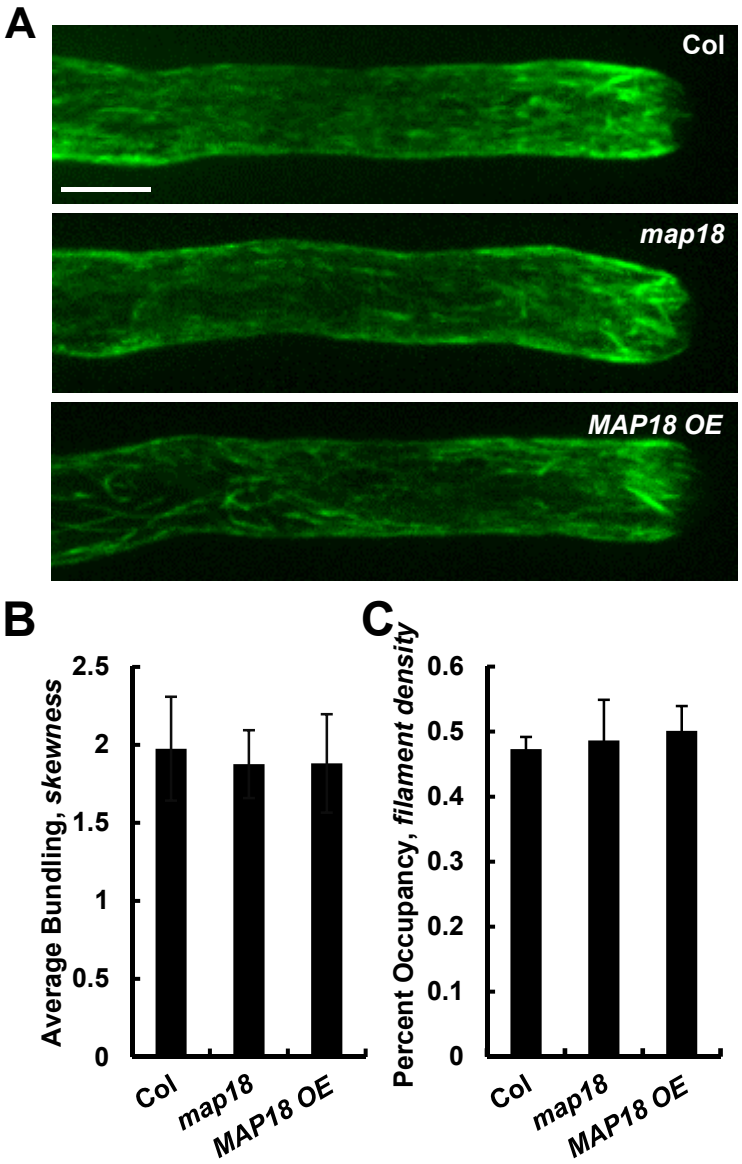
A
Col
map18
MAP18 OE
B
Average Bundling, skewness
2.5
2
1.5
1
0.5
0
Col
map18
MAP18 OE
C
Percent Occupancy, filament density
0.6
0.5
0.4
0.3
0.2
0.1
0
Col
map18
MAP18 OE

Supplemental Figure S4. Microtubules organization in *map18* mutant and *MAP18* overexpression growing root hairs.

Microtubules was visualized in growing root hairs using expressed *GFP-MBD* and observed using spinning disc confocal microscopy.

A, In wild-type, *map18* mutant, and *MAP18* overexpression growing root hairs, microtubules were all organized as bundles along the longitudinal axis in the shank region; short microtubule fragments were observed at sub-apical region and few microtubules were detected in the apical domain. All images are projections of Z-stacks. Bar =10 μm.

B, Quantification of microtubule organization in wild-type, *map18* mutant, and *MAP18* overexpression growing root hairs. There is no significant difference in terms of microtubule bundling (indicated by the average skewness value) among wild-type, *map18* mutant, and *MAP18* overexpression growing root hairs. Data represent the mean ± SD from at least ten growing root hairs for each line.

C, There is no significant difference in terms of percentage occupancy of microtubules (indicated by the average filament density) among wild-type, *map18* mutant, and *MAP18* overexpression growing root hairs. Data represent the mean ± SD from at least ten growing root hairs for each line.

Figure S5

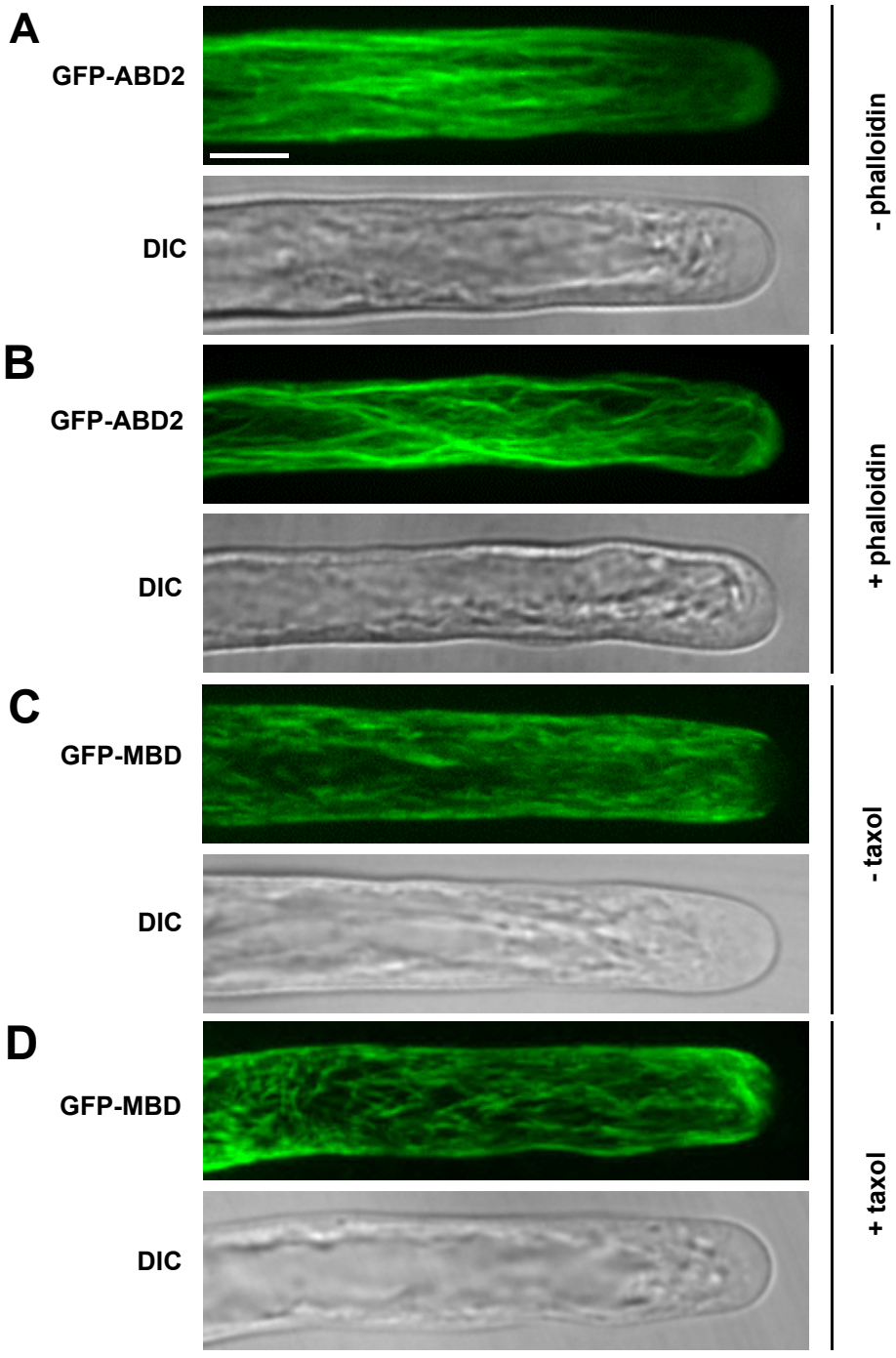
A
GFP-ABD2
DIC
- phalloidin
B
GFP-ABD2
DIC
+ phalloidin
C
GFP-MBD
DIC
- taxol
D
GFP-MBD
DIC
+ taxol

Supplemental Figure S5. Short time treatment with taxol or phalloidin which cause microtubules or F-actin bundling but not induce phenotypic changes of root hairs.

A, Actin organization was visualized in growing root hairs using expressed *GFP-fABD2-GFP* and observed using spinning disc confocal microscopy. Axial actin cables are arranged longitudinally in the shanks of wild-type growing root hairs.

B, The actin filaments cables protrude into the tip region in a growing wild-type root hair after treatment with 3 μM phalloidin for 60 minutes.

C, Microtubules was visualized in growing root hairs using expressed *GFP-MBD* and observed using spinning disc confocal microscopy. Microtubule arrangement mostly longitudinal in a growing root hair.

D, Some thick bundles of microtubules are observed after treated with 7 μM taxol for 60 minutes.

DIC images show no effect of drug treatment on cell shape of root hair for short time.

More than 50 root hairs from at least ten growing roots were observed for each treatment and representative images are presented. All fluorescence images are projections of scanning laser sections (0.5 μm) of Z-stacks and DIC images are single scanning laser sections (0.5 μm). Bar = 10 μm in (A) for (A) to (D).

Figure S6

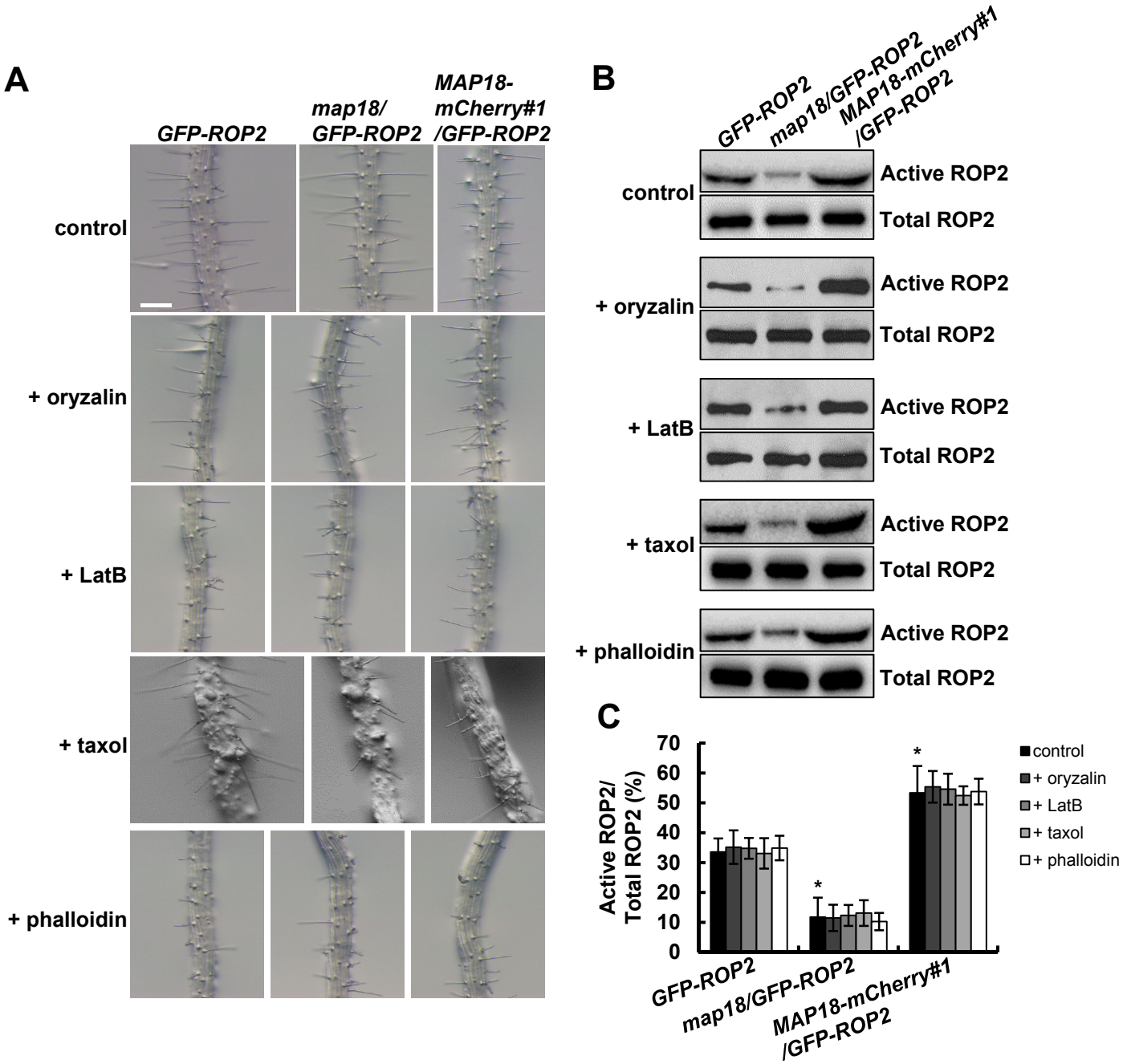
A
GFP-ROP2
map18/ GFP-ROP2
MAP18-mCherry#1 /GFP-ROP2
control
+ oryzalin
+ LatB
+ taxol
+ phalloidin
B
GFP-ROP2
map18/GFP-ROP2
MAP18-mCherry#1 /GFP-ROP2
control
+ oryzalin
+ LatB
+ taxol
+ phalloidin
Active ROP2
Total ROP2
C
Active ROP2/ Total ROP2 (%)
70
60
50
40
30
20
10
0
*
*
control
+ oryzalin
+ LatB
+ taxol
+ phalloidin
GFP-ROP2
map18/GFP-ROP2
MAP18-mCherry#1 /GFP-ROP2

Supplemental Figure S6. MAP18 regulation of ROP2 activity is likely independent of microtubules or F-actin.

A, Representative images of root hair morphologies of five-day-old seedlings treated with various drug for one day were shown. All four drug treatment induced short and branched root hair growth defect in *GFP-ROP2*, *map18/GFP-ROP2*, and *MAP18-mCherry#1/GFP-ROP2* liens. Bar = 1 mm.

B, In a pull-down assay, active GFP-ROP2 was analyzed after treatment with oryzalin, LatB, taxol or phalloidin. Stabilization or Disturbance of microtubules or actin filaments did not obviously affect the respective ROP2 activities in *map18/GFP-ROP2* and *MAP18-mCherry#1/GFP-ROP2* lines.

C, Quantitative analysis of data from (B). ROP2 activity level was determined as the amount of GTP-bound ROP2 versus the amount of total GFP-ROP2. ROP2 activity significantly decreased in *map18/GFP-ROP2* and increased in *MAP18-mCherry#1/GFP-ROP2* lines, regardless of various drug treatment. Data are mean values from five independent experiments ± SD. Asterisk (*) indicates significant difference at $P < 0.05$, ANOVA analysis.

Figure S7

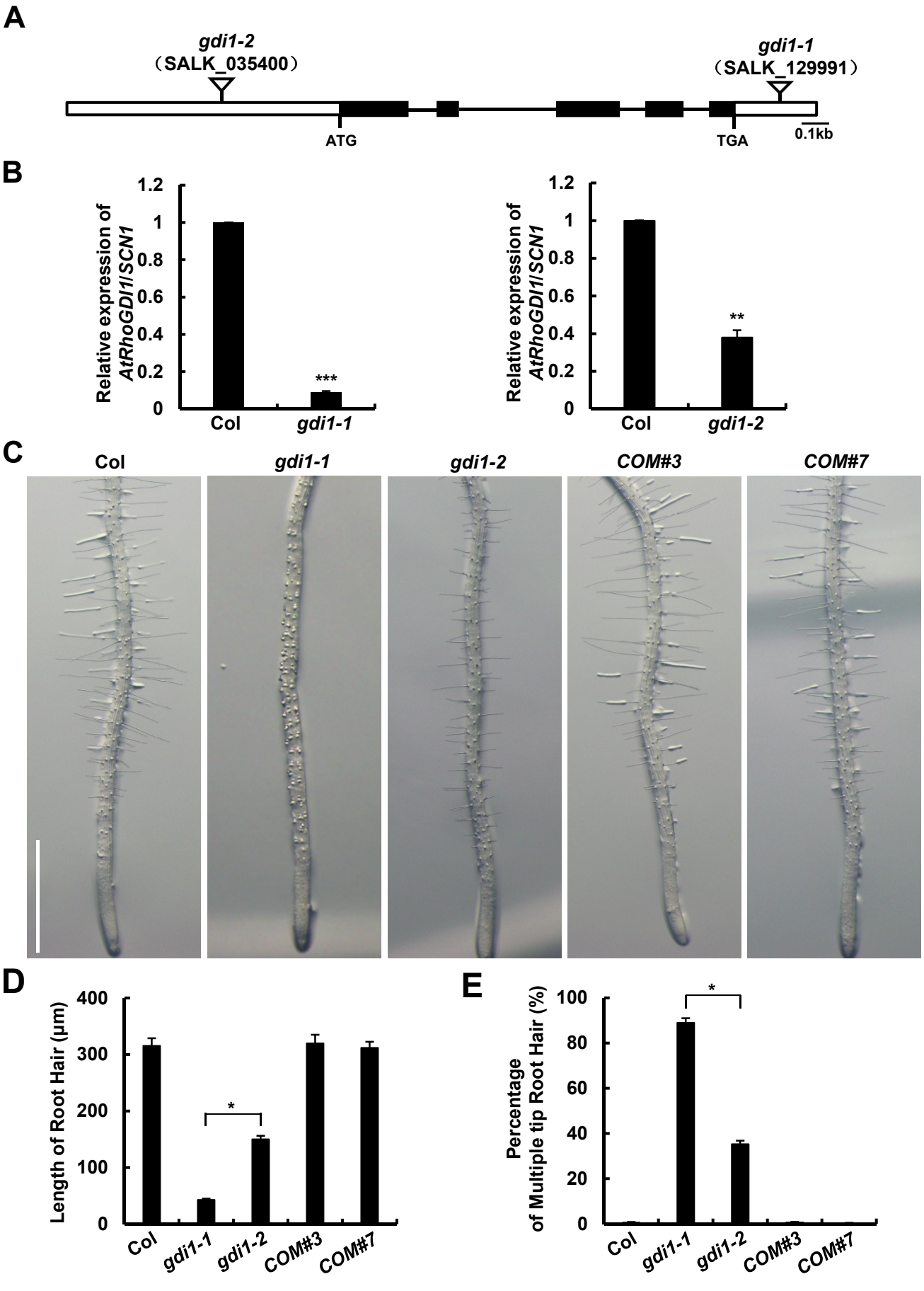
A
gdi1-2
（SALK_035400）
gdi1-1
（SALK_129991）
ATG
TGA
0.1kb
B
Relative expression of AtRhoGDI1/SCN1
1.2
1
0.8
0.6
0.4
0.2
0
***
Col
gdi1-1
Relative expression of AtRhoGDI1/SCN1
1.2
1
0.8
0.6
0.4
0.2
0
**
Col
gdi1-2
C
Col
gdi1-1
gdi1-2
COM#3
COM#7
D
Length of Root Hair (μm)
400
300
200
100
0
*
Col
gdi1-1
gdi1-2
COM#3
COM#7
E
Percentage of Multiple tip Root Hair (%)
100
80
60
40
20
0
*
Col
gdi1-1
gdi1-2
COM#3
COM#7

Supplemental Figure S7. Isolation of *gdi1* knockdown and knockout mutants.

A, SALK_035400 indicates a SALK T-DNA homozygous knockdown line for At3g07880 (*AtRhoGDI1*/*SCN1*), which termed as *gdi1-2*. SALK_129991 indicates a SALK T-DNA homozygous knockout line which termed as *gdi1-1*. Schematic view of the genomic structure of *AtRhoGDI1*/*SCN1* and the site of T-DNA insertion. The black box represents the exon, and the line represents intron. The T-DNA insert (open triangle) is located in the promoter region or 3'UTR of *AtRhoGDI1*/*SCN1*.

B, qRT-PCR analysis demonstrates that *AtRhoGDI1*/*SCN1* transcripts were strongly decreased in *gdi1-1* mutant and also obviously decreased in *gdi1-2* mutant. Data represent the mean ± SD from at least three repeats. Relative amounts of gene expression were normalized to those of *EF1α*. **p < 0.01, ***p < 0.001 by Student's *t*-test.

C, Representative images of root hairs in wild-type, *gdi1-1*, *gdi1-2* line, complemented lines *COM#3* for *gdi1-1*, and *COM#7* for *gdi1-2*. The short and branching phenotypic defects of root hairs of *gdi1-1* and *gdi1-2* were both rescued following transformation with *AtGDI1promotor::GDI1* construct in *COM#3* and *COM#7*, respectively. Bar = 1 mm.

D, Quantitative analysis of the average root hair length of various lines. The root hair length of *gdi1-1* was shorter than that of *gdi1-2* mutant, and both *gdi1-1* and *gdi1-2* root hairs was much shorter than that of wild-type.

E, Quantitative analysis of multiple tip root hairs in various lines. Percentage of branched root hairs was higher in *gdi1-1* and *gdi1-2* mutants than that of wild-type.

More than 150 root hairs from at least twenty growing roots for each line were measured. Data are presented as mean ± SD (Standard Deviation), asterisk (*) indicates significant difference at p < 0.05, ANOVA analysis.

Figure S8

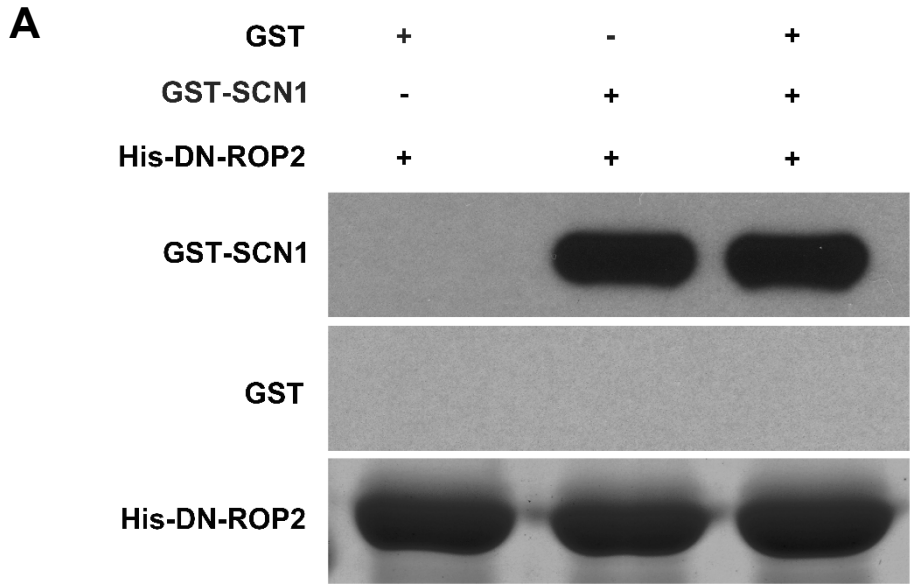
A
GST + - +
GST-SCN1 - + +
His-DN-ROP2 + + +
GST-SCN1
GST
His-DN-ROP2

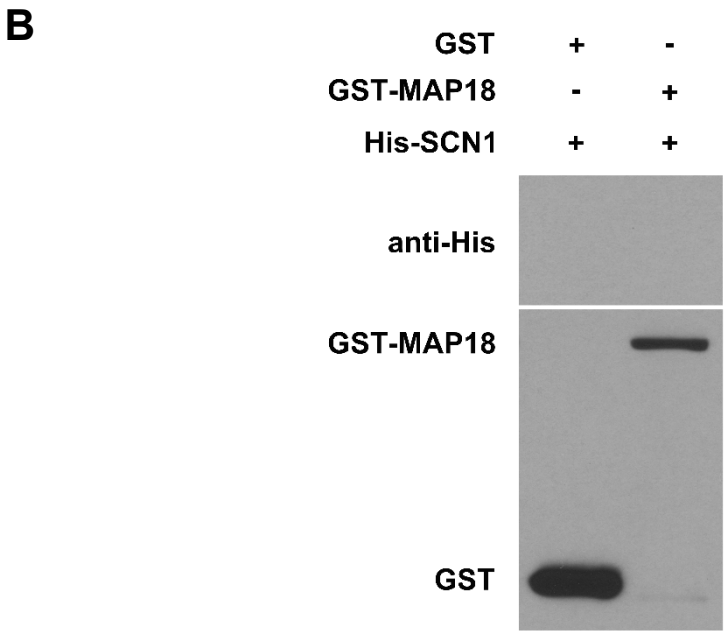
B
GST + -
GST-MAP18 - +
His-SCN1 + +
anti-His
GST-MAP18
GST

Supplemental Figure S8. MAP18 does not interact with AtRhoGDI1/SCN1 in vitro.

A, GST does not affect the combination of GST-SCN1 and His-DN-ROP2. Western blot analysis of pull down shows GST-SCN1 bound with His-DN-ROP2. Then GST protein was incubated together with the two former, and the interaction of GST-SCN1 and His-DN-ROP2 had no change. Experiments were repeated at least three times and a representative result was shown.

B, Western blot analysis of pull down shows His-SCN1 does not interacting with GST-MAP18 as the bait. Anti-His antibody was used for detection. Non-fused GST was used as a negative control for GST-MAP18. Experiments were repeated at least three times and a representative result is shown.

Figure S9

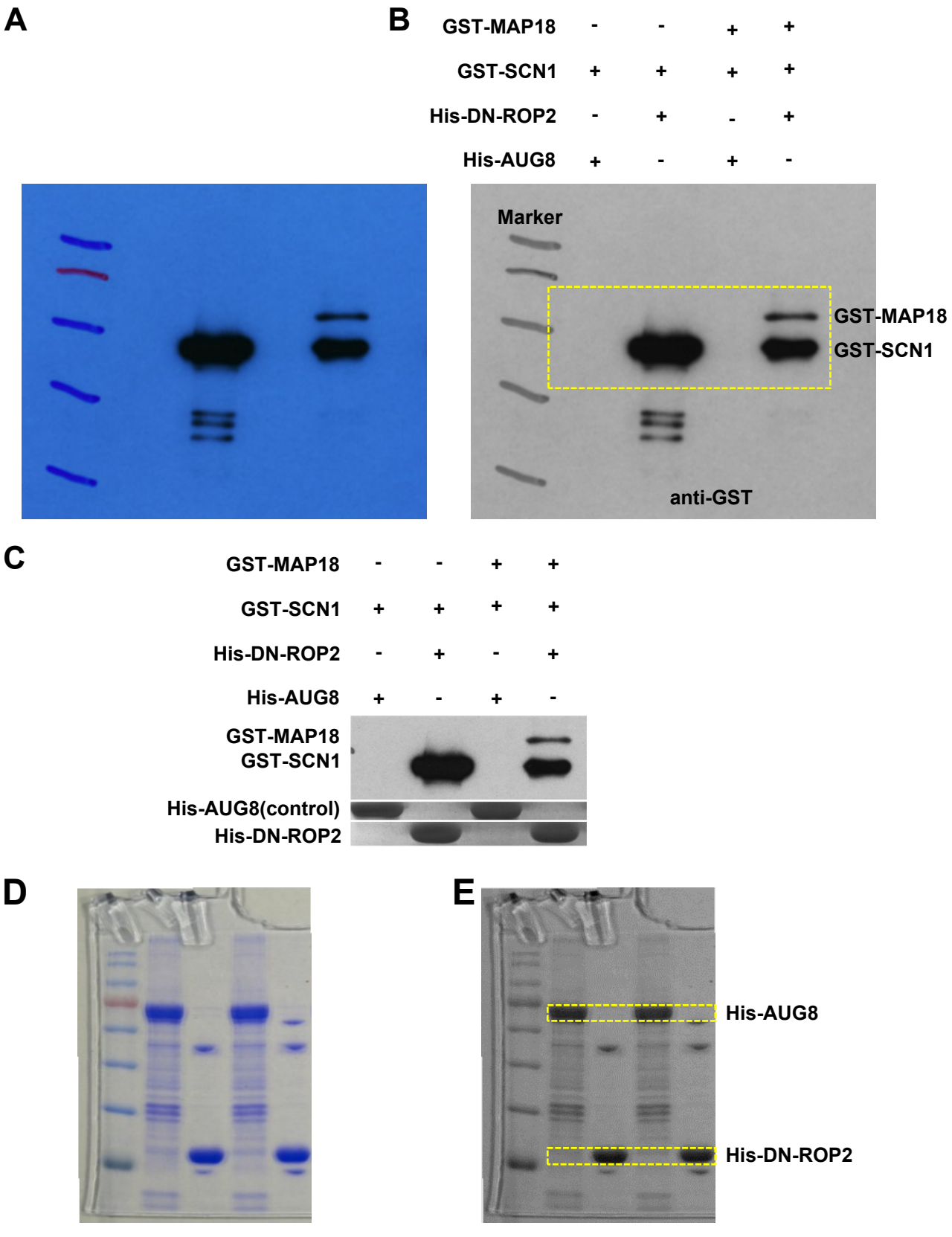
A
B
GST-MAP18 - - + +
GST-SCN1 + + + +
His-DN-ROP2 - + - +
His-AUG8 + - + -
Marker
GST-MAP18
GST-SCN1
anti-GST
C
GST-MAP18 - - + +
GST-SCN1 + + + +
His-DN-ROP2 - + - +
His-AUG8 + - + -
GST-MAP18
GST-SCN1
His-AUG8(control)
His-DN-ROP2
D
E
His-AUG8
His-DN-ROP2

Supplemental Figure S9. The original full size image of Fig. 6C.
Pull down analysis shows GST-SCN1 and GST-MAP18 both could bind with His-DN-ROP2.

Boxes outlined with yellow dots are selected sections from the original blotting or SDS-PAGE, which formed the Fig. 6C (shown in center) together.

Figure S10

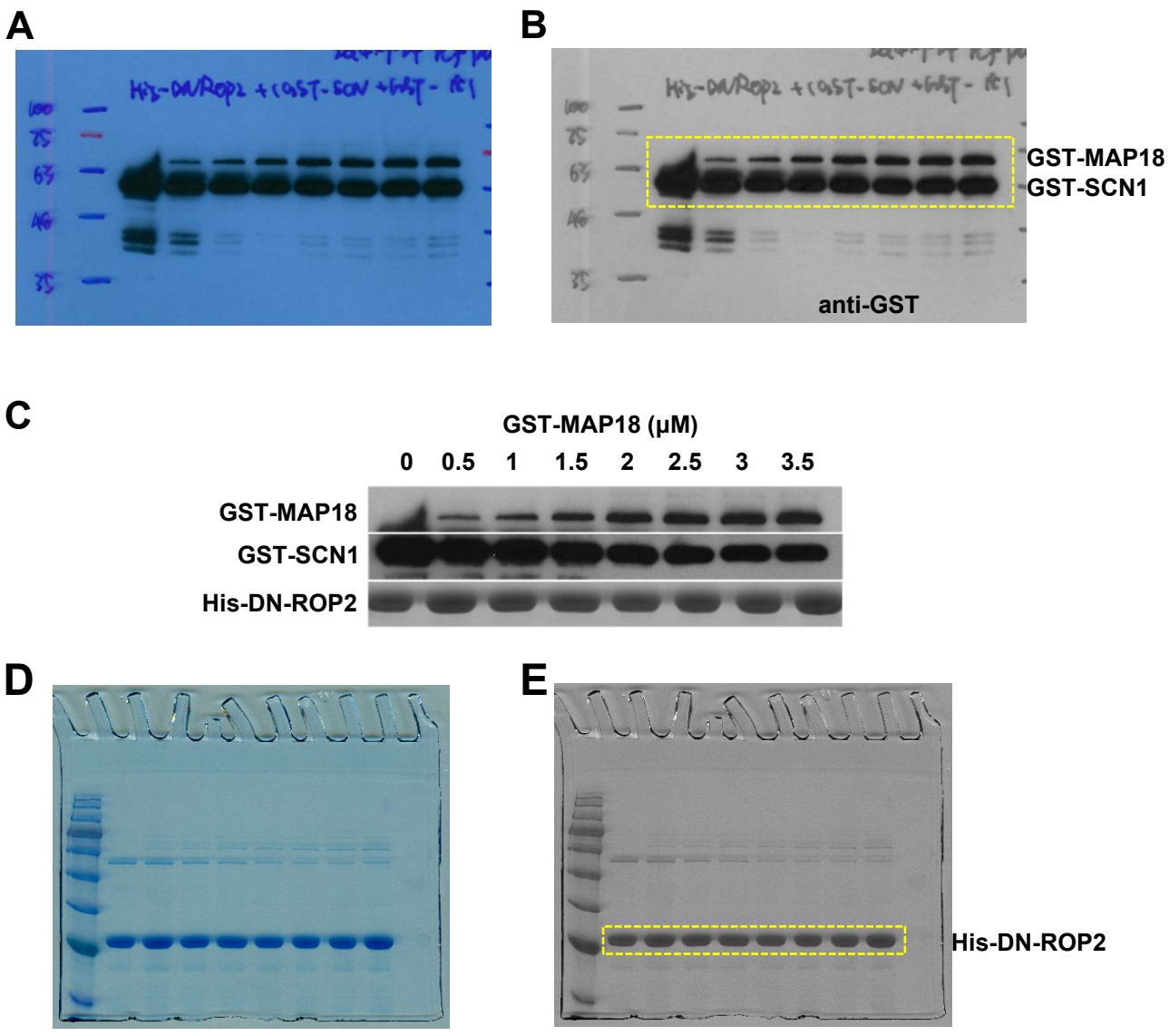
A
B
GST-MAP18
GST-SCN1
anti-GST
C
GST-MAP18 (μM)
0 0.5 1 1.5 2 2.5 3 3.5
GST-MAP18
GST-SCN1
His-DN-ROP2
D
E
His-DN-ROP2

Supplemental Figure S10. The original full size image of Fig. 6G. His-DN-ROP2 was incubated with various concentrations of recombinant GST-MAP18.

Because the GST-SCN1 protein band in 0 uM lane of the below panel in original Fig. 6F ran to the top panel in the blotting. We provide the original full size image here. Boxes outlined with yellow dots are selected sections from the original blotting or SDS-PAGE, which formed the original Fig. 6F (shown in center) together.

Further, we have replaced the image of blotting with a new one of Fig. 6F in revised manuscript, named in new order as Fig. 6G. And quantification analysis of Fig. 6G has also been changed in Fig. 6H.

Figure S11

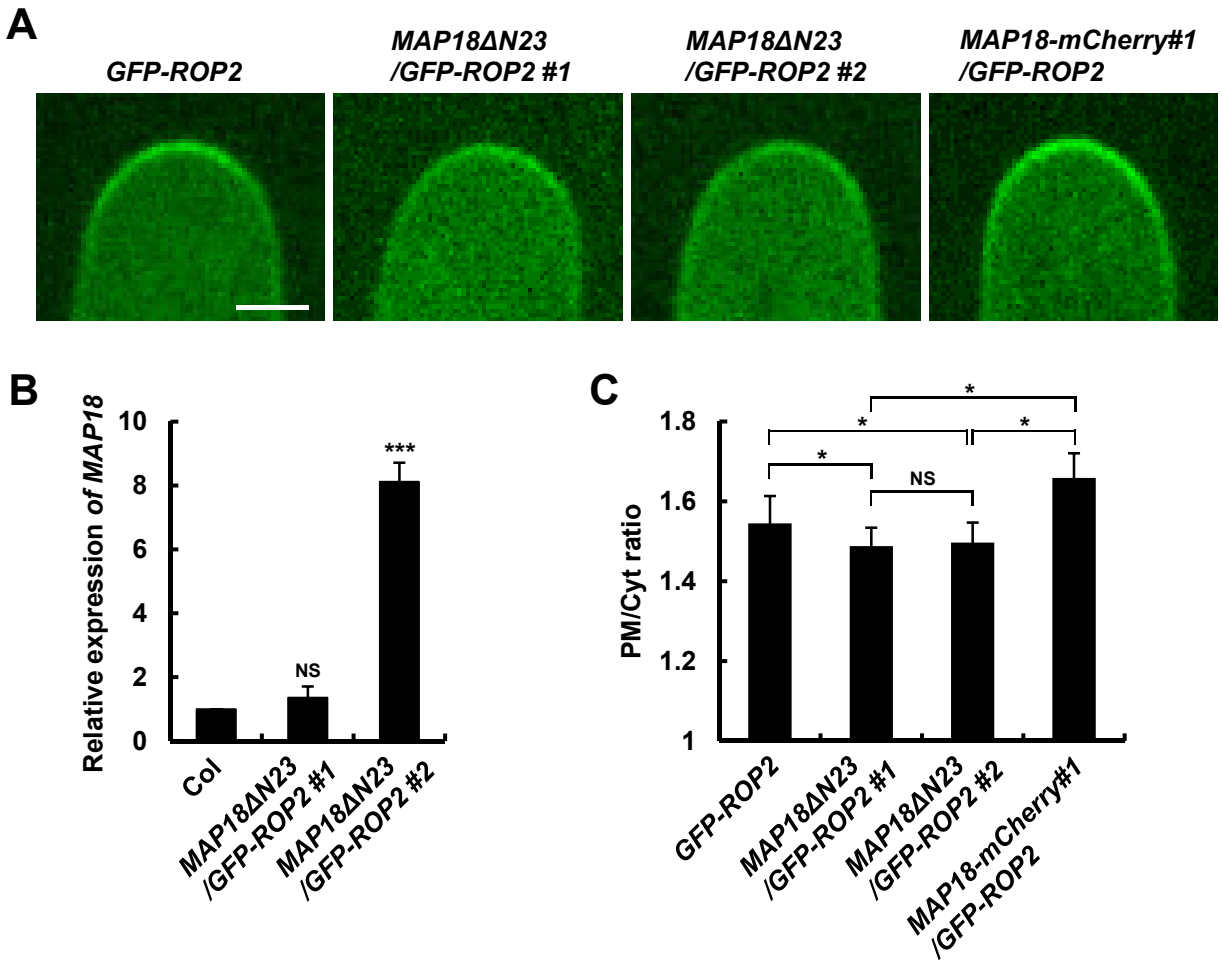
A
GFP-ROP2
MAP18ΔN23 /GFP-ROP2 #1
MAP18ΔN23 /GFP-ROP2 #2
MAP18-mCherry#1 /GFP-ROP2
B
Relative expression of MAP18
10
8
6
4
2
0
NS
***
Col
MAP18ΔN23 /GFP-ROP2 #1
MAP18ΔN23 /GFP-ROP2 #2
C
PM/Cyt ratio
1.8
1.6
1.4
1.2
1
*
*
*
*
NS
GFP-ROP2
MAP18ΔN23 /GFP-ROP2 #1
MAP18ΔN23 /GFP-ROP2 #2
MAP18-mCherry#1 /GFP-ROP2

Supplemental Figure S11. PM-localized GFP-ROP2 is significantly decreased in *MAP18ΔN23*-overexpressing root hairs.

A, Representative images of growing root hairs expressing GFP-ROP2 in wild-type, *MAP18ΔN23,* or *MAP18-mCherry#1* backgrounds. PM targeting of GFP-ROP2 to the tips of growing root hairs is weakened in *MAP18ΔN23/GFP-ROP2 #1 and MAP18ΔN23/GFP-ROP2 #2*, compared with that in *MAP18-mCherry#1*.Bar = 5 μm.

B, qRT-PCR analysis shows that relative *MAP18ΔN23* transcript levels in the transgenic line *MAP18ΔN23/GFP-ROP2 #2* were higher than in the wild-type, and *#1* was slightly higher than the wild-type. Data represent the mean ± SD from at least three repeats. Relative levels of gene expression were normalized to levels from wild-type plants. NS: not significant. ***$p < 0.001$ by Student's *t*-test.

C, Quantitative analysis of the GFP-ROP2 fluorescence intensity PM/Cyt ratio in wild-type, *MAP18ΔN23,* or *MAP18-mCherry#1* root hair backgrounds. Data were collected from between 36-45 root hairs from 15 roots per data set. NS: not significant. Asterisk (*) indicates significant difference at $p < 0.05$, ANOVA analysis.

Figure S12

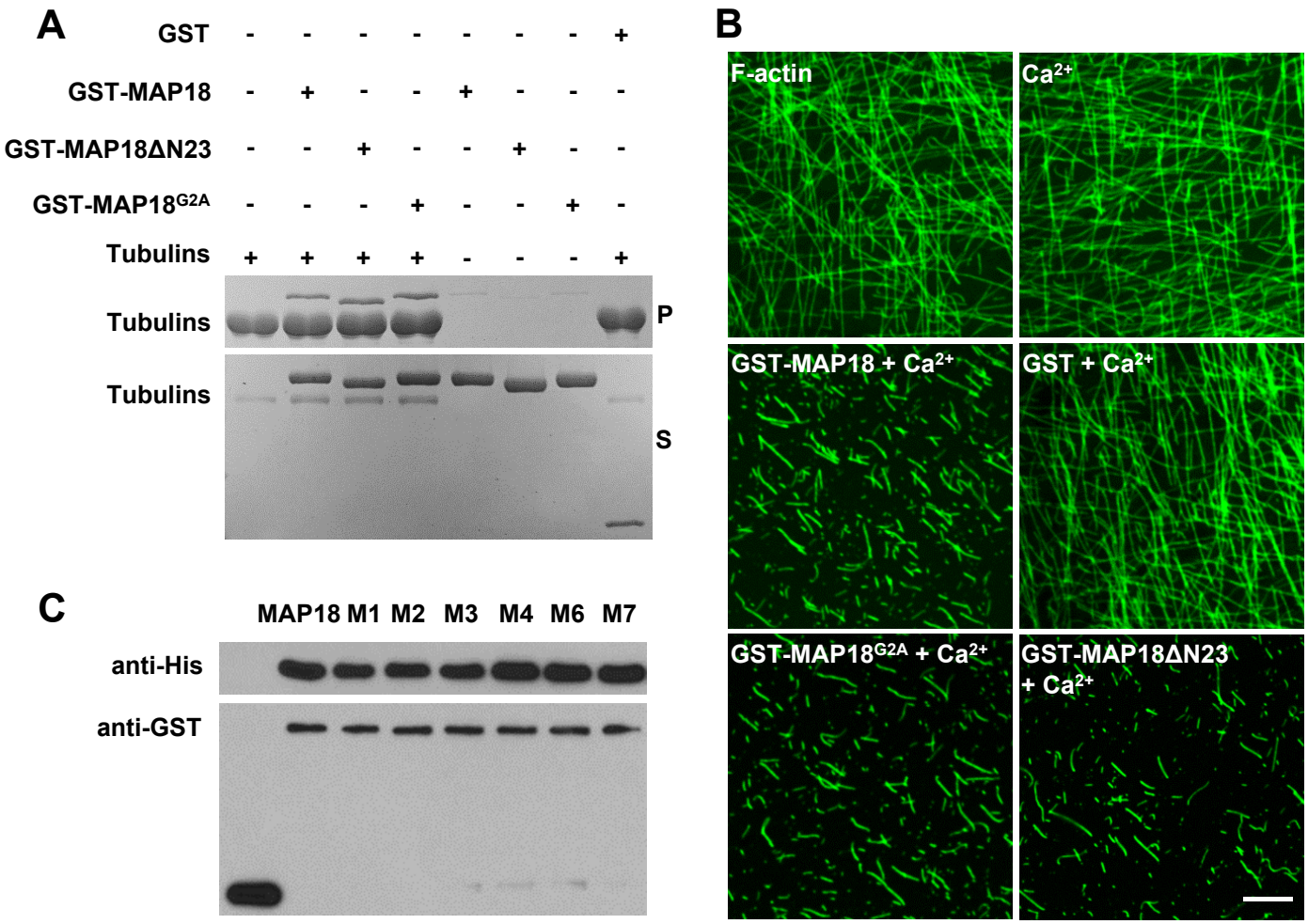
A
GST
GST-MAP18
GST-MAP18ΔN23
GST-MAP18G2A
Tubulins
Tubulins
Tubulins
P
S
B
F-actin
Ca2+
GST-MAP18 + Ca2+
GST + Ca2+
GST-MAP18G2A + Ca2+
GST-MAP18ΔN23 + Ca2+
C
MAP18 M1 M2 M3 M4 M6 M7
anti-His
anti-GST

Supplemental Figure S12. N23 does not influence actin-severing activity and binding microtubules capacity of MAP18.

A, A co-sedimentation assay was performed to assess GST-MAP18, GST-MAP18ΔN23, and GST- MAP18^{G2A} binding to taxol-stabilized polymerized microtubules.

B, Preformed actin filaments (labeled with Alexa 488–phalloidin) are fragmented in the presence of GST-MAP18, GST- MAP18ΔN23, or GST-MAP18^{G2A} together with 50 μM Ca^{2+}. Bar = 5 μm.

C, Pull-down assays were performed to assess the binding of GST-M1~M7 to His-DN-ROP2. All of the mutant proteins of MAP18 bound to His-DN-ROP2 in vitro, whether or not they have the F-actin-severing activity. GST-MAP18 was used as a positive control.

Figure S13

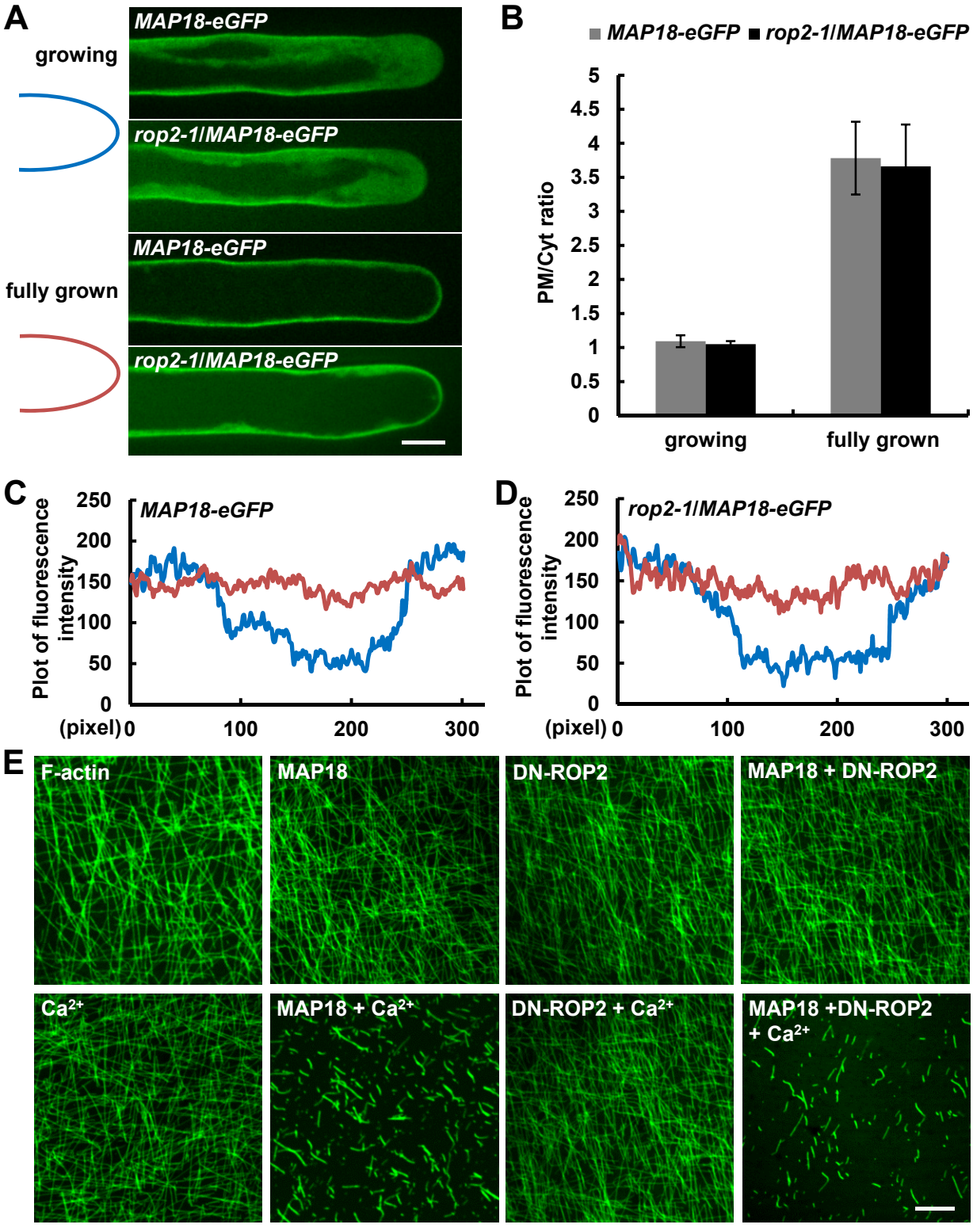
A
growing
MAP18-eGFP
rop2-1/MAP18-eGFP
fully grown
MAP18-eGFP
rop2-1/MAP18-eGFP
B
MAP18-eGFP
rop2-1/MAP18-eGFP
PM/Cyt ratio
5
4.5
4
3.5
3
2.5
2
1.5
1
0.5
0
growing
fully grown
C
MAP18-eGFP
Plot of fluorescence intensity
250
200
150
100
50
0
(pixel) 0
100
200
300
D
rop2-1/MAP18-eGFP
Plot of fluorescence intensity
250
200
150
100
50
0
(pixel) 0
100
200
300
E
F-actin
MAP18
DN-ROP2
MAP18 + DN-ROP2
Ca2+
MAP18 + Ca2+
DN-ROP2 + Ca2+
MAP18 +DN-ROP2 + Ca2+

Supplemental Figure S13. The subcellular localization and F-actin-severing activity of MAP18 are both not regulated by ROP2.

A, Upper panel: MAP18-eGFP localizes to the shank PM and the cytoplasm of the growing root hairs apical region in wild-type (upper) or *rop2-1* mutant background (lower). Lower panel: The MAP18-eGFP signal was observed throughout the entire PM of fully grown root hairs in wild-type (upper) or *rop2-1* mutant background (lower). Bar = 10 μm.

B, Quantification of the PM/Cyt (marked by 1/2 as shown in Figure 3D) fluorescence ratio of MAP18-eGFP at the apex in growing and fully grown root hairs of wild-type or *rop2-1* mutant background. The PM/Cyt ratio of MAP18-eGFP in wild-type is very similar to that in *rop2-1* background. Data represent the mean ± SD of at least 20 measurements based on three independent experiments.

C, Fluorescence intensities (arbitrary units) of MAP18-eGFP along the root hair tip region in growing (blue lines) or fully grown root hair (red lines) in wild-type. The MAP18-eGFP fusion protein localizes to the PM at the shank in the growing root hair, while uniformly distributed in the entire PM, including the apex, in fully grown root hairs.

D, Fluorescence intensities (arbitrary units) of MAP18-eGFP along the root hair tip region in growing (blue lines) or fully grown root hair (red lines) in *rop2-1* mutant. Location pattern of MAP18-eGFP is not altered in *rop2-1* both in growing and fully grown root hairs.

E, Preformed actin filaments (labeled with Alexa 488–phalloidin) remain intact when incubated with 10 nM GST-MAP18, 50 mM Ca^{2+} or His-DN-ROP2 alone. While adding His-DN-ROP2, actin filaments are fragmented in the presence of GST-MAP18 together with 50 mM Ca^{2+}. Bar = 5 μm.

Figure S14

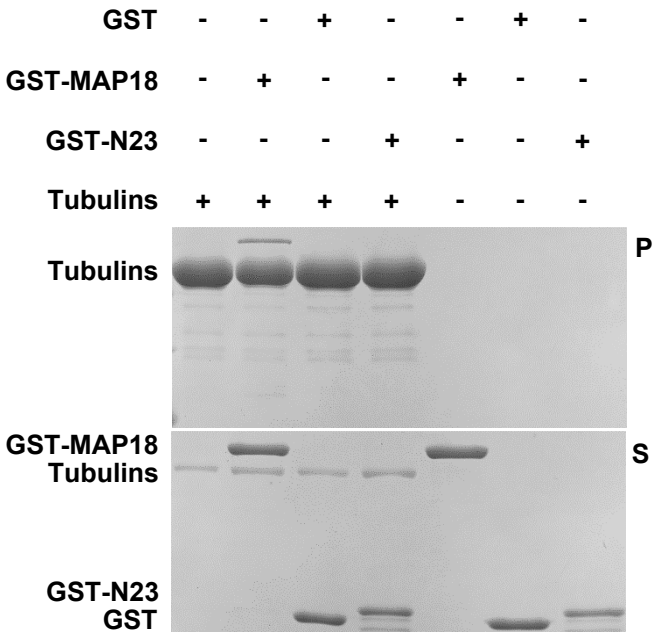
GST - - + - - + -
GST-MAP18 - + - - + - -
GST-N23 - - - + - - +
Tubulins + + + + - - -
Tubulins
P
GST-MAP18
Tubulins
S
GST-N23
GST

Supplemental Figure S14. N23 fragment does not bind to microtubules in vitro.

Recombinant GST-N23 protein does not co-sediment with 5 μM preformed taxol-stabilized microtubules. As a positive control, recombinant MAP18 protein appeared mainly in the supernatant (S) in the absence of microtubules and cosedimented with microtubules into the pellets (P) after centrifugation. Non-fused GST was used as a negative control.

Supplemental Table S1. List of primers used in this study.

Primers name		Pairs of specific primers
gdi1-1-SALK	*gdi1-1*-LP	TGATAGCCTCGCCATCATATC
	gdi1-1-RP	TTGTATCAAGGATCGCGTTTC
gdi1-2-SALK	*gdi1-2*-LP	TTGTACATGATCATGATGGCG
	gdi1-2-RP	CTATTTCTTCCACGCGCATAG
His-CA/DN-ROP2	ROP2-F (BamHI)	GGATCC ATGGCGTCAAGGTTTATAAAGTGT
	ROP2-R (SalI)	GTCGAC TCACAAGAACGCGCAACG
GST-MAP18ΔN23	MAP18ΔN23-F(BamHI)	GGATCC GAAGTTGTTGAGGAGGAGAAGC
	MAP18ΔN23-R (SalI)	GTCGAC TCAAGCCTTTTGTGGCGCAG
GST-MAP18^{G2A}	MAP18^{G2A}-F (BamHI)	GGATCC ATGGCTTATTGGAAGTC
	MAP18^{G2A}-R (SalI)	GTCGAC TCAAGCCTTTTGTGGCGCAG
GST-SCN1	SCN1-F (BamHI)	GGATCC ATGTCTTTGGTATCTGGAGCC
	SCN1-R (EcoRI)	GAATTC TCAAAGCGCAGGCCATTC
His-SCN1	SCN1-F (BamHI)	GGATCC ATGTCTTTGGTATCTGGAGCC
	SCN1-R (HindIII)	AAGCTT TCAAAGCGCAGGCCATTC
RIC4ΔC-GFP	RIC4ΔC-F	ATGAGAGATAGAATGGAGAGACTTG
	RIC4ΔC-R	CGGCGGTATGAGATCTT
BiFC	MAP18-F (BamHI)	GGATCC ATGGGTTATTGGAAGTCGAAG
	MAP18-R (SalI)	GTCGAC AGCCTTTTGTGGCGCAG
	ROP2-F (BamHI)	GGATCC ATGGCGTCAAGGTTTATAAAGTGT
	ROP2-R (SalI)	GTCGAC CAAGAACGCGCAACGGTT
LCI	ROP2-cLuc-F (KpnI)	GGTACC ATGGCGTCAAGGTTTATAAAGTGT
	ROP2-cLuc-R (PstI)	CTGCAG TCACAAGAACGCGCAACG
	MAP18-nLuc-F (BamI)	GGATCC ATGGGTTATTGGAAGTCGAAG
	MAP18-nLuc-R (SalI)	GTCGAC AGCCTTTTGTGGCGCAG
Co-IP	MAP18-F (PstI)	CTGCAG ATGGGTTATTGGAAGTCGAAG
	MAP18-R (KpnI)	GGTACC AGCCTTTTGTGGCGCAG
	SCN1-F (PstI)	CTGCAG ATGTCTTTGGTATCTGGAGCCA
	SCN1-R (KpnI)	GGTACC AAGCGCAGGCCATTCTTTA
	ROP2-F (EcoRI)	GAATTC ATGGCGTCAAGGTTTATAAAGTGT
	ROP2-R (BamHI)	GGATCC TCACAAGAACGCGCAACG
qPCR	MAP18-qPCR-F	CAACCGGCGAGAAAGAGATAG
	MAP18-qPCR-R	CTTCTACGGCTGGCTTCTTC
	ROP2-qPCR-F	CCTGGTGTTCCCATTATCCTTGT
	ROP2-qPCR-R	GATCCAATCAGTTTCTTCAGTTCCTC
	SCN1-qPCR-F	CGAGAAGGACAAGGATGATGAG
	SCN1-qPCR-R	CGGATCAAGAGTCTCTCCAATG
	RIC4ΔC-qPCR-F	TCTCCTCTCTCTAAGCCTCATC
	RIC4ΔC-qPCR-R	GAAACCGCAAGGAACTTGAATAC